

Structural, Electronic, and Magnetic Properties of MnO

J.E. Pask, D.J. Singh, I.I. Mazin, C.S. Hellberg, and J. Kortus

Center for Computational Materials Science, Naval Research Laboratory, Washington, DC 20375

(December 2, 2024)

Abstract

We calculate the structural, electronic, and magnetic properties of MnO from first principles, using the full-potential linearized augmented plane-wave method, with both local-density and generalized-gradient approximations to exchange and correlation. We find the ground state to be of rhombohedrally distorted B1 structure with compression along the $[111]$ direction, antiferromagnetic with type-II ordering, and insulating, consistent with experiment. We show that the distortion can be understood in terms of a Heisenberg model with distance dependent nearest-neighbor and next-nearest-neighbor couplings determined from first principles. Finally, we show that magnetic ordering can induce significant charge anisotropy, and give predictions for electric field gradients in the ground-state rhombohedrally distorted structure.

PACS: 75.30.Et, 75.10.Lp, 75.50.Ee, 76.60.Gv

I. INTRODUCTION

Since the recognition of their unusual insulating and magnetic properties over a half century ago, the first-row transition-metal monoxides have been the subject of much experimental and theoretical interest. Because they are highly correlated Mott or charge-transfer insulators,^{1,2} first-principles theoretical approaches based on density-functional (DFT) in the local-density approximation (LDA)^{3,4} have proven inadequate for understanding certain properties such as electrical conductivity and magnetic moments, and new or extended approaches such as self-interaction corrected (SIC),^{5,6} orbital polarization corrected,⁷ on-site Coulomb corrected (LDA+U),^{8,9} and model GW¹⁰ methods have been developed in order to address these deficiencies. Nevertheless, DFT-LDA based approaches have proven successful in understanding a number of ground-state properties, most notably in the cases of MnO and NiO which are correctly predicted to be insulating and antiferromagnetic with type-II ordering (though the gaps are underestimated).^{11–14} Moreover, the use of the generalized gradient approximation (GGA)¹⁵ has been shown to yield further improvements.¹⁶ Here, we focus on the larger-moment compound, MnO, from the standpoint of DFT in both LDA and GGA approximations.

Above the Néel temperature, $T_N = 118$ K, MnO is a paramagnetic insulator with the rocksalt (B1) structure. Below T_N , it is a type-II antiferromagnetic (AFII, Fig. 1) insulator with rhombohedrally distorted B1 structure. The rhombohedral distortion takes the form of a compression along the [111] direction, taking cubic angles from 90° to 90.62° .¹⁷ Based upon augmented spherical wave (ASW) LDA calculations, Oguchi *et al.*^{12,13} showed that the electronic structure is very sensitive to the magnetic ordering, and that the LDA can predict MnO to be an insulator, but only when the magnetic ordering is AFII, as it is experimentally. Based again upon ASW-LDA calculations, Terakura *et al.*¹⁴ subsequently explained the stability of the AFII ordering relative to nonmagnetic (NM), ferromagnetic (FM), and type-I antiferromagnetic (AFI) orderings in terms of the strong $dd\sigma$ coupling through the oxygens of opposite-spin cation sublattices in the AFII ordering vs. same-spin sublattices in the AFI ordering. Using a linearized augmented planewave (LAPW) approach, Dufek *et al.*¹⁶ showed that the GGA can yield further improvements to LDA results, finding a minor improvement of the gap from 1.0 eV to 1.4 eV and of the Mn spin magnetic moments from $3.72\mu_B$ to $4.15\mu_B$, relative to experimental values of 3.6–3.8 eV and 4.58 – $4.79\mu_B$, respectively. Using a linear combination of atomic orbitals (LCAO) Hartree-Fock (HF) approach, Towler *et al.*¹⁸ calculated structural, magnetic, elastic, and vibrational properties. They determined the correct AFII ground state and a rhombohedral distortion angle of 90.47° , very close to the experimental value. Mackrodt *et al.*¹⁹ subsequently applied the same methodology to the calculation of phase transitions under pressure. Using a linear muffin tin orbital (LMTO) GGA approach, Cohen *et al.*²⁰ subsequently calculated low- and high-pressure properties of MnO in the context of an investigation of magnetic moment collapse at high pressure. More recently, using a planewave (PW) GGA approach, supplemented by LDA+U calculations, Fang *et al.*²¹ investigated low- and high-pressure properties. They determined the correct AFII ground state, a rhombohedral distortion angle of $\approx 92^\circ$, somewhat larger than the experimental value, magnetic moments, and a phase transition to a metallic NiAs structure at high pressure. Massidda *et al.*²² have investigated magnetic-order-induced anisotropies in linear-response properties using a combination of *ab initio* and model calculations. In

the course of their study, they determined a ground-state distortion angle of 90.66° , very close to the experimental value, and showed that the zone-center optic phonon frequencies and Born effective charge tensor exhibit significant magnetic-order-induced anisotropies, even when assuming the perfect rocksalt structure, contrary to the assumption of cubic symmetry commonly made in interpreting experimental data.

The mechanism underlying the rhombohedral distortion below T_N was examined by Kanamori²³ in the late 1950's. Based upon paramagnetic susceptibility data, it was concluded that there are significant exchange interactions between nearest-neighbor (NN) cations and, based upon Curie-Weiss and Néel temperature data, that these interactions are predominantly direct in nature. It was further concluded, consistent with earlier suggestions of Greenwald and Smart,²⁴ that the rhombohedral distortion below T_N is due to these direct NN interactions. Assuming distance dependent NN and next-nearest-neighbor (NNN) coupling, Rodbell and Owen²⁵ subsequently used a molecular field approach to derive an expression for the distortion in terms of these couplings which supported the above conclusions, having explicit dependence only upon the NN coupling. Lines and Jones²⁶ subsequently deduced the same expression from a Heisenberg model containing only NN and NNN couplings, and used a Green's function approach²⁷ in the random phase approximation to evaluate the exchange constants based upon susceptibility data. More recently, Oguchi *et al.*^{12,13} have calculated coupling constants from *ab initio* ASW-LDA calculations, employing the Korringa-Kohn-Rostoker coherent potential approximation (KKR-CPA). In this work it was shown that couplings beyond NNN were in fact negligible, justifying the assumption made almost universally in previous work. The constants obtained, however, were about three times larger than those deduced from experiment. Among the reasons suggested for the discrepancy were the assumption that total-energy differences were well represented by eigenvalue-sum differences, and spherical approximations in the ASW and KKR-CPA calculations.

Here, we calculate the structural, electronic, and magnetic properties of MnO by the full-potential linearized augmented planewave method, using both LDA and GGA approximations to exchange and correlation, thus improving upon spherical, pseudopotential, and/or strictly LDA approximations in previous work. We examine the rhombohedral distortion in terms of a Heisenberg model with distance dependent NN and NNN interactions determined from *ab initio* calculations without spherical approximations, using ordered structures rather than the CPA. Finally, we consider the charge anisotropy induced by magnetic ordering through *ab initio* calculations of electric field gradients.

II. CRYSTAL, ELECTRONIC, AND MAGNETIC STRUCTURE

General potential LAPW²⁸ calculations were carried out for NM, FM, AFI, and AFII magnetic orderings. Well converged basis sets were employed with a planewave cutoff of 18.9 Ry, corresponding to an average of ≈ 109 basis functions per atom (the exact number being \mathbf{k} -dependent).³⁰ Local orbital extensions were used for Mn $l = 1, 2, 3$ and O $l = 1, 2$ channels to include higher lying semi-core states and relax linearization errors. Core states were treated fully relativistically in a self-consistent atomic-like approximation, while valence states were treated scalar relativistically. Increasing the planewave cutoff to 24.7

Ry, corresponding to an average of ≈ 159 basis functions per atom, yielded a change in total energy of less than 2.5 mRy/atom in LDA tests. Highly converged special \mathbf{k} point sets³¹ were employed consisting of 512 points in the rhombohedral (NM, FM, and AFII) Brillouin zones and 486 points in the tetragonal (AFI) zone. Doubling the number of \mathbf{k} points in each direction yielded a change in total energy of less than 0.15 mRy/atom in LDA tests. LDA and GGA calculations employed the exchange-correlation functionals of Hedin and Lundqvist,³² and Perdew and Wang,³³ respectively. As shown in Fig. 2, the LDA calculations predict the ground state to be antiferromagnetic with AFII ordering, consistent with experiment¹⁷ and previous calculations^{14,18,21} by other methods. The GGA results are qualitatively similar, predicting the correct AFII ground state, but with a lattice constant of 8.38 a.u., much improved from the LDA value of 8.16 a.u. relative to the experimental value of 8.38 a.u.³⁴

Figures 3 and 4(c) show the Brillouin zone and LDA band structure and density of states corresponding to the ground-state AFII ordering. The GGA results are qualitatively similar, but with a larger exchange splitting and gap of ≈ 0.29 Ry and ≈ 0.105 Ry, respectively, compared to LDA values of ≈ 0.27 Ry and ≈ 0.075 Ry, due to lower occupied and higher unoccupied d states relative to O p states. In both cases, the large exchange splitting and narrow e_g band are sufficient to produce an insulator, consistent with experiment¹⁷ and previous calculations^{14,18,21} by other methods. Significantly, however, both LDA and GGA calculations predict other configurations to be metallic (Figs. 4(a),(b)), with the implication that the spin-disordered paramagnetic state would also be metallic, contrary to experiment. Our results are thus consistent with the characterization of MnO as a correlated Mott-Hubbard insulator.

III. RHOMBOHEDRAL DISTORTION

Figure 5 shows LDA results for the total energy vs. rhombohedral strain in the ground-state AFII ordering at the experimental volume. The GGA results are essentially the same. The rhombohedral strain is determined by a parameter g through the volume conserving strain tensor

$$G = \begin{pmatrix} 1+g & g & g \\ g & 1+g & g \\ g & g & 1+g \end{pmatrix} (1+3g)^{-1/3}.$$

As shown in the figure, the calculations predict the ground state to be slightly compressed ($g < 0$) along the [111] direction. A least squares fit of the results yielded minimizing strains of $g = -0.01456$ and $g = -0.01465$, corresponding to deviations of 1.68° and 1.69° from the 90° cubic angle for LDA and GGA calculations, respectively. A comparison with experiment and previous calculations by other methods is shown in Table I. Both LDA and GGA results overestimate the experimental angle somewhat, consistent with recent PW-GGA calculations²¹ but inconsistent with a recent LAPW-LDA calculation.²² Hartree-Fock calculations,¹⁸ which produce larger gaps, underestimate the distortion somewhat. Within simple tight-binding pictures, interatomic exchange interactions are inversely related to the gap ($\sim t^2/I$ or $\sim t^2/U$, where t is a hopping parameter and I and U are on-site interactions

related to the size of the gap). As discussed below, the distortion is driven by the variation of NN exchange with distance, so the tendency to overestimate the distortion may reflect the incomplete treatment of Hubbard correlations and resulting small gaps associated with LDA and GGA approximations.

The compression along [111] can be understood in terms of a Heisenberg Hamiltonian with distance dependent NN and NNN interactions:

$$H = \sum_{NN} J_1 \mathbf{S}_i \cdot \mathbf{S}_j + \sum_{NNN} J_2 \mathbf{S}_i \cdot \mathbf{S}_j. \quad (1)$$

Considering a single formula unit, the above Hamiltonian reduces to

$$H^{\text{FM}} = (6J_1 + 3J_2)S^2, \quad (2)$$

$$H^{\text{AFI}} = (-2J_1 + 3J_2)S^2, \quad (3)$$

and

$$H^{\text{AFII}} = -3J_2S^2, \quad (4)$$

where S is the magnitude of the cation spin, for FM, AFI, and AFII orderings, respectively. We deduce the exchange constants from the above expressions and *ab initio* total energies for each ordering at the experimental volume, with $S = 5/2$. Our results are shown in Table II, along with previous *ab initio* ASW-KKR-CPA^{12,13} and semi-empirical^{26,35,36} results for comparison. While there are still significant differences, our *ab initio* results agree in sign and order of magnitude with the semi-empirical ones, and are generally closer to the semi-empirical ones than previous *ab initio* results employing the CPA and spherical approximations, implying better consistency with thermal and spin-wave data. In any case, we find both NN and NNN couplings to be antiferromagnetic, consistent with the Goodenough-Kanamori rules^{12,37} and previous results. We note that since these calculations involve energy differences on the order of a few mRy, large \mathbf{k} point sets were required in order to attain sufficient convergence. The above results were calculated using 4096 special \mathbf{k} points in the full zone. Reduction of this set to 1728 points yielded differences of less than 0.003 mRy and 0.001 mRy for J_1 and J_2 , respectively, in LDA tests. Convergence with respect to planewave cutoff was also checked. Increasing the cutoff from 18.9 Ry to 24.7 Ry, yielded a difference of less than 0.002 mRy for both J_1 and J_2 in LDA tests. Calculated Mn moments varied by less than 2.2% over all magnetic orderings in both LDA and GGA tests.

We deduce the distance dependence of the interactions from calculations on distorted structures. For a small compression along [111], adjacent-plane NNs move closer together while in-plane NNs move farther apart, so that $J_1 \rightarrow J'_1$ for adjacent-plane NNs while $J_1 \rightarrow J''_1$ for in-plane NNs; while, for a volume conserving strain, NNN distances remain unchanged to first order.²⁵ Considering again a single formula unit, the above Hamiltonian (1) reduces to

$$H^{\text{FM}} = (3J'_1 + 3J''_1 + 3J_2)S^2, \quad (5)$$

$$H^{\text{AFI}} = (-J'_1 - J''_1 + 3J_2)S^2, \quad (6)$$

and

$$H^{\text{AFII}} = (-3J'_1 + 3J''_1 - 3J_2)S^2 \quad (7)$$

for FM, AFI, and AFII orderings, respectively. We deduce the exchange constants as before from the above expressions and *ab initio* total energies corresponding to the appropriate magnetic orderings, at the experimental volume and distortion. Our results are shown in Table II, along with semi-empirical values for comparison. As the table shows, our *ab initio* results predict the same distance dependence as the semi-empirical ones: whatever the nature of the NN coupling, whether direct or indirect, its strength decreases with distance on the relevant distance scale, as may be expected.

The observed compression along [111] now follows straightforwardly from the above established distance dependence and antiferromagnetic nature of the interactions. For a small compression angle $\delta > 0$,

$$J'_1 = J_1(1 + c\delta),$$

$$J''_1 = J_1(1 - c\delta),$$

and, for a volume conserving strain, J_2 remains unchanged to first order; where $J_1 > 0$ (antiferromagnetic NN interactions) and $c > 0$ (strength decreases with distance) as established above. Thus, for the AFII structure,

$$H^{\text{AFII}}_{\text{strained}} - H^{\text{AFII}}_{\text{unstrained}} = -6S^2 J_1 c \delta < 0;$$

and so the compression lowers energy. Physically, for a small compression, the antiparallel-spin NNs move closer together while the parallel-spin NNs move farther apart, while NNN distances remain unchanged. And so, since the NN interaction is antiferromagnetic and decreases with distance, the energy is lowered. Thus, while decisive in determining the magnetic ordering,¹⁴ the strong NNN coupling through the oxygens has nothing (to first order) to do with the observed rhombohedral distortion. Rather, it is the weaker antiferromagnetic NN coupling which plays the decisive role.

IV. MAGNETIC-ORDER-INDUCED CHARGE ANISOTROPY

The electric field gradient (EFG) tensor, defined as the second derivative of the Coulomb potential at the atomic position,³⁸ provides a sensitive probe of the electronic charge distribution; and due to this sensitivity, very accurate distributions are required in order to calculate EFGs reliably. Blaha *et al.*³⁹ were the first to show that the LAPW method could be used to calculate accurate EFGs with no adjustable parameters. In subsequent work⁴⁰ it was shown that, due to the extreme sensitivity of the EFGs to inaccuracies in the density, the local orbital extension of the method (LAPW+LO),²⁹ as we employ here, is sometimes required in order to obtain reliable results.

Massidda *et al.*²² have investigated magnetic-order-induced anisotropies of two nonmagnetic (spin-independent) linear-response properties of MnO, finding significant anisotropies

in the zone-center optic phonon frequencies and Born effective charge tensor despite the fact that the atomic positions had cubic symmetry, so that the only noncubic ingredient was in the spin channel. Since strong Hubbard correlations are thought to separate charge and spin degrees of freedom in general, measurements of such couplings in comparison with density-functional calculations can be particularly illuminating. Here, we consider magnetic-order-induced anisotropy in a static, nonmagnetic quantity: the charge density itself. Since the EFG (the largest-magnitude eigenvalue of the EFG tensor) depends sensitively on the charge density and vanishes for cubic symmetry, it provides a sensitive measure of such anisotropy. And using this measure, our calculations show that magnetic ordering can induce significant charge anisotropy in MnO—on the order of that associated with noncubic crystal structure in some cases. Table III shows our LDA and GGA results for MnO in various magnetic and structural conformations. Cubic AFI and AFII structures show significant (up to $\approx 1.3 \times 10^{21}$ V/m²) EFGs, indicating significant anisotropy due solely to the magnetic ordering, with an order of magnitude difference in the Mn EFGs in the AFI and AFII orderings. The last row of Table III corresponds to the AFII structure with the observed rhombohedral distortion, and so constitutes our prediction for the observed EFGs. These values should be amenable to experimental measurement and, as mentioned, comparison with density-functional predictions should prove quite useful.

V. SUMMARY AND CONCLUSIONS

We have calculated the structural, electronic, and magnetic properties of MnO from first principles, using the LAPW method, with both LDA and GGA approximations to exchange and correlation. In both the LDA and GGA we found the ground state to be of rhombohedrally distorted B1 structure with compression along the [111] direction, antiferromagnetic with AFII ordering, and insulating, consistent with experiment and previous calculations by other methods. The GGA was shown to yield a much improved lattice constant. However, highly converged LDA and GGA results were shown to overestimate the observed rhombohedral distortion, consistent with one recent calculation but inconsistent with others. We showed that the distortion can be understood in terms of a Heisenberg model with distance dependent NN and NNN couplings determined from first principles, obtaining exchange constants in better agreement with semi-empirical values than previous *ab initio* results employing the CPA and spherical approximations, but still somewhat larger in general. Whereas the NNN coupling plays the decisive role in determining the magnetic ordering, it was shown that the weaker NN coupling plays the decisive role in the structural distortion. Finally, we showed that magnetic ordering can induce significant charge anisotropy, on the order of that associated with noncubic structure in some cases, and gave density-functional predictions for EFGs in the ground-state rhombohedrally distorted structure.

ACKNOWLEDGMENTS

Support from the Office of Naval Research and National Research Council is gratefully acknowledged.

REFERENCES

- ¹ J. Zaanen, G.A. Sawatzky, and J.W. Allen, Phys. Rev. Lett. **55**, 418 (1985).
- ² A. Fujimori, N. Kimizuka, T. Akahane, T. Chiba, S. Kimura, F. Minami, K. Siratori, M. Taniguchi, S. Ogawa, and S. Suga, Phys. Rev. B **42**, 7580 (1990); A.E. Bocquet, T. Mizokawa, T. Saitoh, H. Namatame, A. Fujimori, *ibid.* **46**, 3771 (1992).
- ³ P. Hohenberg and W. Kohn, Phys. Rev. **136**, B864 (1964); W. Kohn and L.J. Sham, Phys. Rev. **140**, A1133 (1965).
- ⁴ *Theory of the Inhomogeneous Electron Gas*, edited by S. Lundqvist and N.H. March (Plenum, New York, 1983).
- ⁵ A. Svane and O. Gunnarsson, Phys. Rev. Lett. **65**, 1148 (1990).
- ⁶ Z. Szotek, W.M. Temmerman, and H. Winter, Phys. Rev. B **47**, 4029 (1993).
- ⁷ M.R. Norman, Phys. Rev. B **44**, 1364 (1991).
- ⁸ V.I. Anisimov, J. Zaanen, and O.K. Andersen, Phys. Rev. B **44**, 943 (1991).
- ⁹ J. Hugel and M. Kamal, Solid State Commun. **100**, 457 (1996).
- ¹⁰ S. Massidda, A. Continenza, M. Posternak, and A. Baldereschi, Phys. Rev. Lett. **74**, 2323 (1995).
- ¹¹ T.M. Wilson, Int. J. Quantum Chem. Symp. **3**, 757 (1970).
- ¹² T. Oguchi, K. Terakura, and A.R. Williams, Phys. Rev. B **28**, 6443 (1983).
- ¹³ T. Oguchi, K. Terakura, and A.R. Williams, J. Appl. Phys. **55**, 2318 (1984).
- ¹⁴ K. Terakura, T. Oguchi, A.R. Williams, and J. Kübler, Phys. Rev. B **30**, 4734 (1984).
- ¹⁵ D.C. Langreth and J.P. Perdew, Phys. Rev. B **15**, 2884 (1977); *ibid.* **21**, 5469 (1980).
- ¹⁶ P. Dufek, P. Blaha, V. Sliwko, and K. Schwarz, Phys. Rev. B **49**, 10170 (1994).
- ¹⁷ D. Seino, Phys. Rev. B **38**, 11901 (1988).
- ¹⁸ M.D. Towler, N.L. Allen, N.M. Harrison, V.R. Saunders, W.C. Mackrodt, and E. Aprà, Phys. Rev. B **50**, 5041 (1994).
- ¹⁹ W.C. Mackrodt, E.-A. Williamson, D. Williams, and N.L. Allan, Phil. Mag. B **77**, 1063 (1998).
- ²⁰ R.E. Cohen, I.I. Mazin, and D.G. Isaak, Science **275**, 654 (1997).
- ²¹ Z. Fang, I.V. Solovyev, H. Sawada, and K. Terakura, Phys. Rev. B **59**, 762 (1999).
- ²² S. Massidda, M. Posternak, A. Baldereschi, and R. Resta, Phys. Rev. Lett. **82**, 430 (1999).
- ²³ J. Kanamori, Prog. Theor. Phys. **17**, 197 (1957).
- ²⁴ S. Greenwald and J.S. Smart, Nature **166**, 523 (1950).
- ²⁵ D.S. Rodbell and J. Owen, J. Appl. Phys. **35**, 1002 (1964).
- ²⁶ M.E. Lines and E.D Jones, Phys. Rev. **139**, A1313 (1965).
- ²⁷ M.E. Lines, Phys. Rev. **139**, A1304 (1965).
- ²⁸ S.H. Wei and H. Krakauer, Phys. Rev. Lett. **55**, 1200 (1985); S.H. Wei, H. Krakauer, and M. Weinert, Phys. Rev. B **32**, 7792 (1985), and references therein.
- ²⁹ D. Singh, Phys. Rev. B **43**, 6388 (1991).
- ³⁰ Sphere radii of 2.07 a.u. and 1.61 a.u. were used for Mn and O atoms, respectively.
- ³¹ A. Baldereschi, Phys. Rev. B **7**, 5212 (1973); D.J. Chadi and M.L. Cohen, *ibid.* **8**, 5747 (1973); H.J. Monkhorst and J.D. Pack, *ibid.* **13**, 5188 (1976); **16**, 1748 (1977).
- ³² L. Hedin and B.I. Lundqvist, J. Phys. C **4**, 2064 (1971).
- ³³ J.P. Perdew, in *Electronic Structure of Solids 1991*, edited by P. Ziesche and H. Eschrig

(Akademie Verlag, Berlin, 1991); J.P. Perdew and Y. Wang, Phys. Rev. B **45**, 13224 (1992).

³⁴ L.F. Mattheiss, Phys. Rev. B **5**, 290 (1972).

³⁵ M. Kohgi, Y. Ishikawa, and Y. Endoh, Solid State Commun. **11**, 391 (1972).

³⁶ G. Pepy, J. Phys. Chem. Solids **35**, 433 (1974).

³⁷ See, e.g., P.W. Anderson, in *Solid State Physics*, edited by F. Seitz and D. Turnbull (Academic, New York, 1963), Vol. 14, p. 99.

³⁸ For a review, see M.H. Cohen and F. Reif, in *Solid State Physics*, edited by F. Seitz and D. Turnbull (Academic, New York, 1957), Vol. 5, p. 322.

³⁹ P. Blaha, K. Schwarz, and P. Herzig, Phys. Rev. Lett. **54**, 1192 (1985).

⁴⁰ P. Blaha, D.J. Singh, P.I. Sorantin, and K. Schwarz, Phys. Rev. B **46**, 1321 (1992).

FIGURES

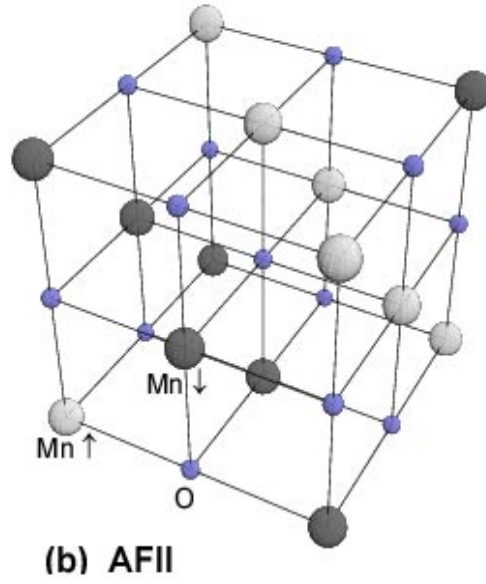
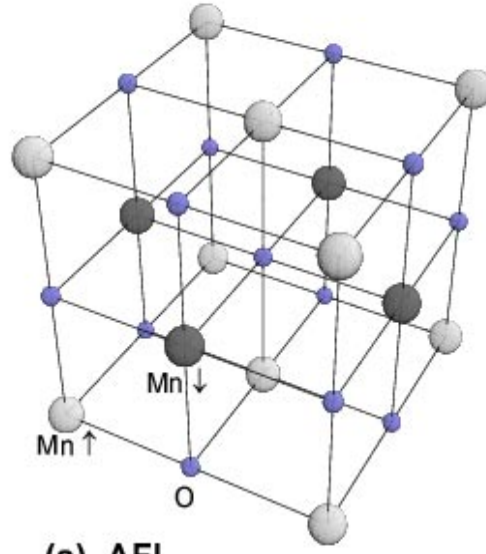


FIG. 1. (a) AFI ($[001]$) and (b) AFII ($[111]$) magnetic orderings.

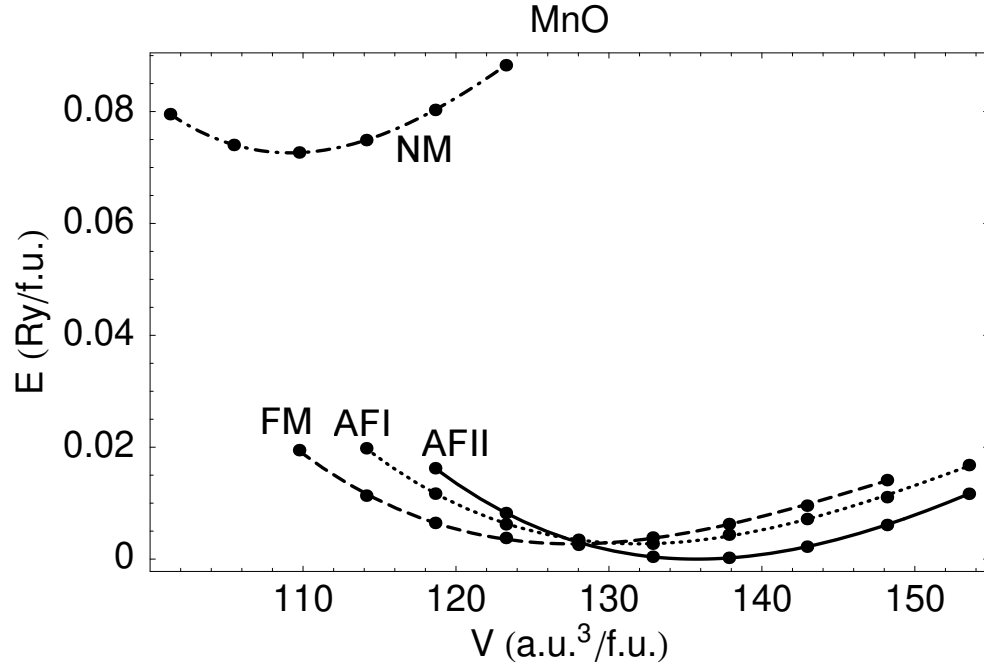
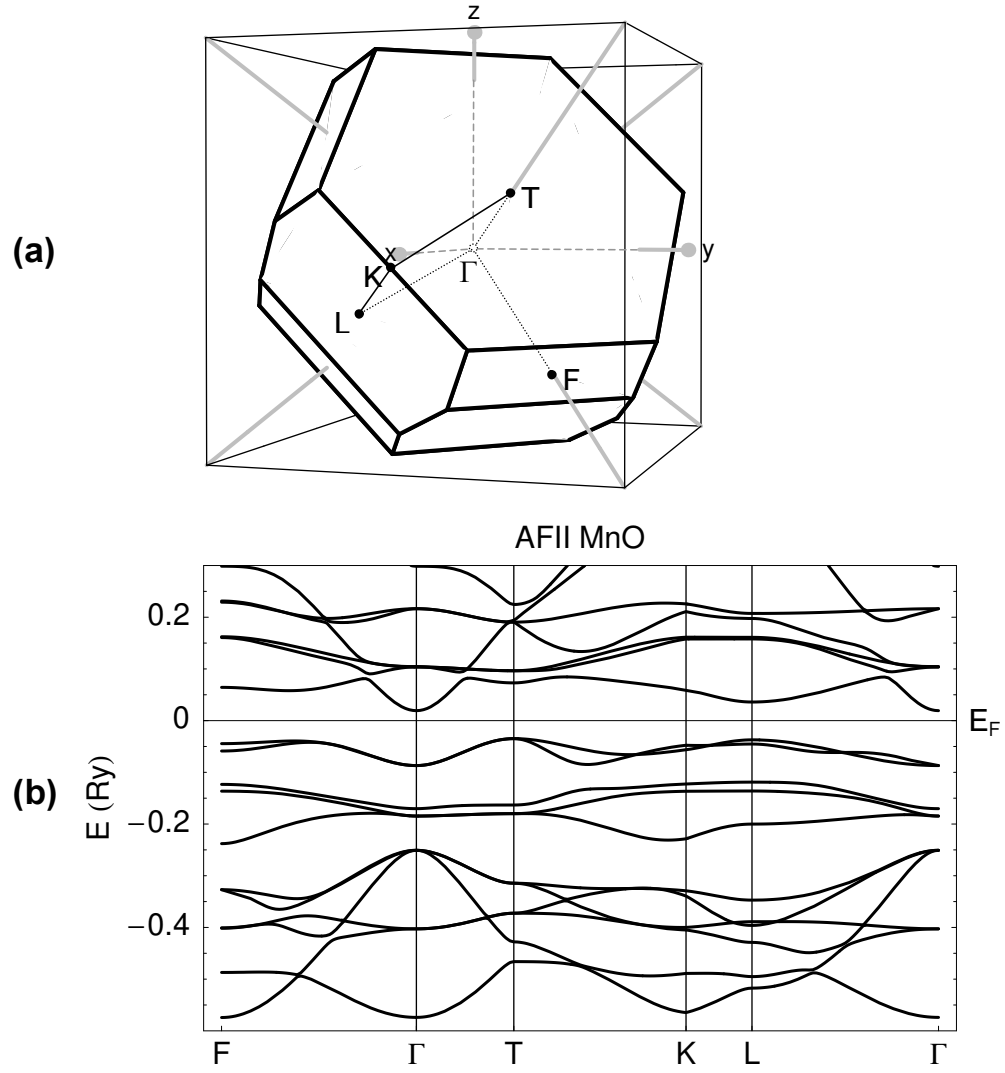


FIG. 2. LAPW-LDA results for energy vs. volume of MnO, predicting AFII ground-state magnetic ordering.



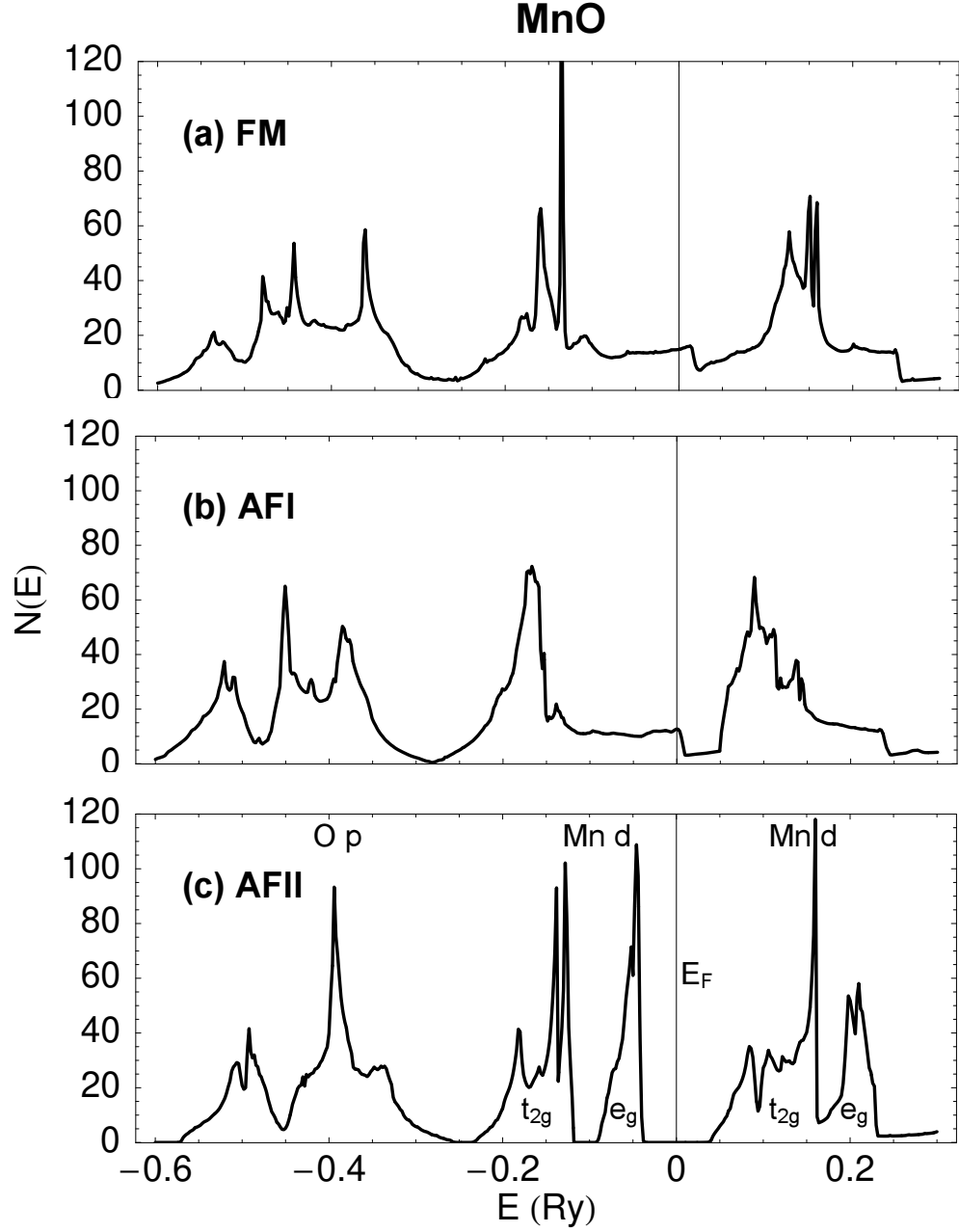


FIG. 4. LAPW-LDA density of states for (a) FM, (b) AFI, and (c) AFII MnO. Only the AFII ordering is predicted to be insulating.

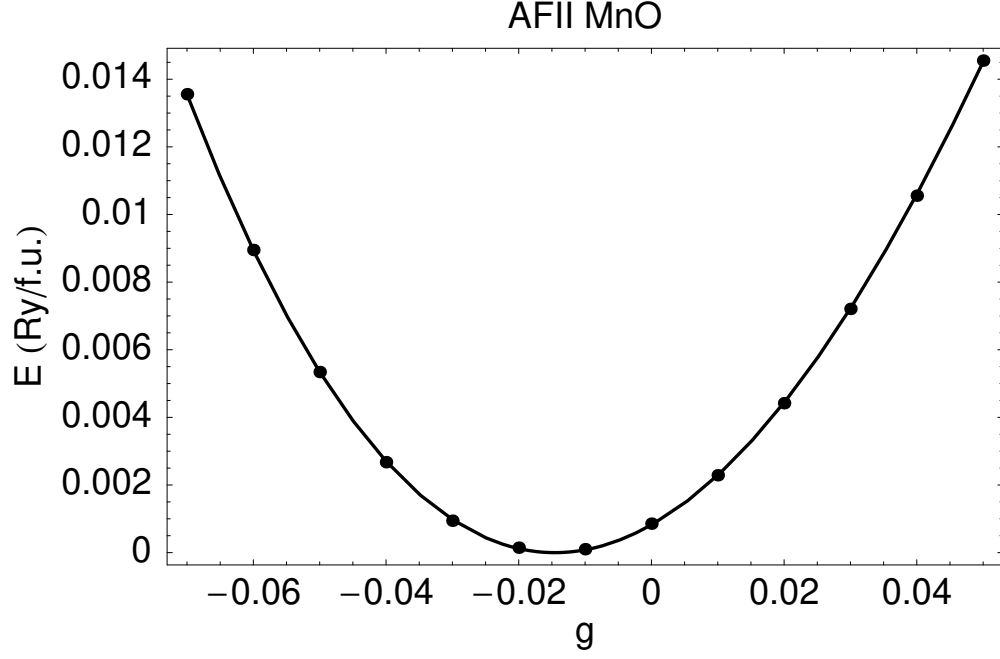


FIG. 5. LAPW-LDA energy vs. rhombohedral strain for AFII MnO at the experimental volume. The minimizing strain of $g = 0.01456$ corresponds to a deviation of 1.68° from the ideal cubic angle.

TABLES

TABLE I. LAPW LDA and GGA rhombohedral distortion angles for AFII MnO, and comparison to previous calculations and experiment.

LAPW		PW-GGA	LCAO-HF	LAPW-LDA	EXPT
LDA	GGA	(Ref. 21)	(Ref. 18)	(Ref. 22)	(Ref. 17)
1.68°	1.69°	$\approx 2.0^\circ$	0.47°	0.66°	0.62°

TABLE II. Exchange constants (in K) for MnO based on LAPW LDA and GGA calculations, and comparison to other *ab initio* and semi-empirical results.

	LAPW		ASW-KKR-CPA	Semi-emp	Semi-emp	Semi-emp
	LDA	GGA	(Refs. 12,13)	(Ref. 26)	(Ref. 35)	(Ref. 36)
J_1	9.8	18.8	30	10	8.9	8.5
J_2	24.5	33.0	30	11	10.3	9.6
J'_1	12.3	21.3			10.0	9.9
J''_1	7.4	16.4			7.9	7.5

TABLE III. LAPW LDA and GGA EFGs (in 10^{21} V/m²) for various conformations of MnO. The last row corresponds to the observed rhombohedrally distorted ground state. The asymmetry parameters vanish in all cases.

		LDA	GGA
AFI:	Mn	1.31	0.65
	O	0.18	0.13
AFII:	Mn	-0.13	-0.05
	O	0.22	0.27
AFII (distorted):	Mn	0.10	0.20
	O	-0.12	-0.08